Spectroscopic study of ^{40}K

Rozina Rahaman,[1] Abhijit Bisoi ◉,[1,*] Ananya Das,[2] Y. Sapkota ◉,[3] Arkabrata Gupta ◉,[1] S. Ray,[4] S. Sarkar ◉,[1] Yashraj ◉,[5] A. Sharma ◉,[6] Bharti Rohila ◉,[7] I. Ahmed,[5] Kaushik Katre,[5] S. Dutt,[5] S. Kumar,[5] R. P. Singh ◉,[5] R. Kumar,[5] and S. Muralithar[5]

[1]*Indian Institute of Engineering Science and Technology, Shibpur, Howrah 711103, India*
[2]*Dream Institute of Technology, Samali, Kolkata 700104, India*
[3]*Assam Don Bosco University, Tapesia Campus, Sonapur, Assam 782402, India*
[4]*Amity Institute of Nuclear Science and Technology, Noida, Uttar Pradesh 201313, India*
[5]*Inter-University Accelerator Centre, New Delhi 110067, India*
[6]*Department of Physics, Himachal Pradesh University, Shimla, Himachal Pradesh 171005, India*
[7]*Department of Physics, Panjab University, Chandigarh 160014, India*

High spin states of ^{40}K populated through the ^{27}Al(^{19}F, αnp)^{40}K reaction at 68 MeV beam energy were studied using the Indian National Gamma Array (INGA) facility. Six new levels and fourteen new transitions were added to the existing level scheme. The spins and parities of most of the levels were assigned, modified, or confirmed from R_{DCO}, R_{ADO}, and linear polarization measurements. The multipole mixing ratios (δ) for most of the transitions were measured. Large-basis shell-model calculations were performed to understand the microscopic origin of the levels. Different particle restrictions in sd and pf shell orbitals were used to explain the experimental results.

I. INTRODUCTION

Nuclei in the neighborhood of the doubly closed $N = Z = 20$ region generally show the characteristics of spherical single-particle excitations [1] and their excitation spectra are well explained by the spherical shell model [2–9]. However, in the Nilsson diagram, the low Ω orbitals from the pf shell, especially for $1f_{7/2}$, are sharply downsloping for increasing deformation. Therefore, one may expect deformed or superdeformed structures with multihole multiparticle configurations in the sd shell nuclei. The advancement of detection and data acquisition systems made it possible to study the spectroscopic properties of light nuclei at high spins. As a result, several deformed, even superdeformed (SD) bands have been observed in nuclei around ^{40}Ca, which has generated new interest in this mass region. Gerace and Green *et al.* [10] explained in their early work about the low-lying levels of ^{40}Ca as a mixture of spherical and deformed states formed by raising particles from the sd to the pf shell. Later, a superdeformed (SD) band was identified by Ideguchi *et al.* in ^{40}Ca, which is generated by 8p-8h excitation [11]. A weakly deformed ground-state band and highly deformed slightly triaxial sideband in ^{42}Ca were reported in Ref. [12]. SD bands were identified also in a few Ar isotopes, viz. ^{36}Ar [13], ^{38}Ar [14], and ^{40}Ar [15,16]. The origin of the observed SD band in ^{36}Ar was explained by the $(s_{1/2}d_{3/2})^4(pf)^4$ configuration [13]. Shell-model calculation shows that the band in ^{38}Ar was generated from 4p-6h excitations [14]. Similarly, for ^{40}Ar, the origin of the SD band was explained by the mixing of different mp-mh ($m = 0, 2, 4$) configurations [15,16]. Therefore, this region gives a unique opportunity to investigate experimentally the interplay between single-particle and collective modes of excitations and interpret them theoretically by using microscopic large-basis shell-model calculations.

^{40}K is an odd-odd ($N = 21$, $Z = 19$) nucleus and lies in the lower pf shell. In the recent past, we investigated the high-spin structure of a few upper sd shell nuclei, viz., ^{33}S [5], ^{34}Cl [6], ^{35}Cl [7], ^{37}Ar [8], and ^{38}K [9]. The low-lying states of these nuclei are primarily generated from single-particle excitations. However, at higher excitation energy, the signature of collective excitation has been found. ^{40}K is the isobaric partner nucleus of ^{40}Ar and ^{40}Ca where the existence of collectivity in terms of deformed and superdeformed bands has already been reported [11,15,16]. So, one may also expect collective excitations at higher excitation energy in ^{40}K, generated from multiparticle multihole excitations.

The ^{40}K nucleus was previously studied by Soderstrom *et al.* [17] through heavy-ion reactions. They extended the level scheme of ^{40}K up to 8 MeV by adding a few new levels and γ's. The spin and parity of all the newly added levels up to 7 MeV were tentative. They assigned them based on the comparison of the branching ratios to the Weisskopf estimates. They added three more levels above 7 MeV but their spins and parities were not assigned. Our primary motivation is, therefore, to investigate the high-spin structure of ^{40}K and search for collective excitations at high excitation energy in ^{40}K. Our preliminary work on ^{40}K was already reported in Ref. [18].

*abhijitbisoi@physics.iiests.ac.in

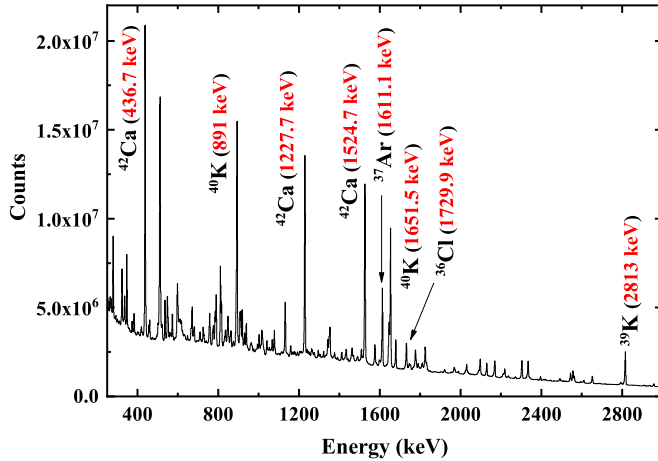FIG. 1. A total projection spectrum of γ rays emitted from different nuclei populated in the present experiment.
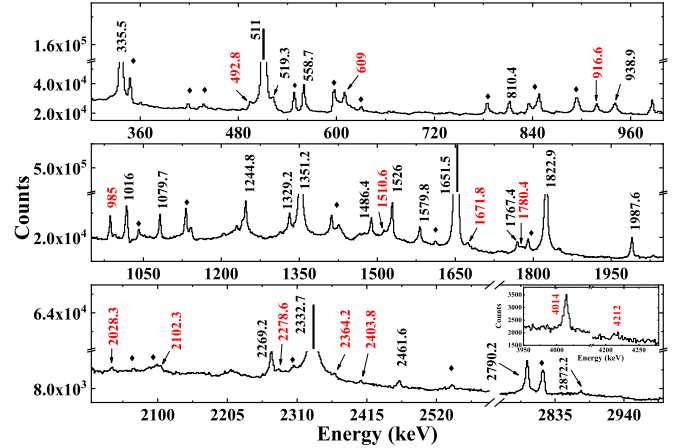

FIG. 2. Background subtracted coincidence spectrum obtained by putting a gate on the 891 keV transition. Newly observed transitions are shown by red color. Transitions marked with ♦ are from contaminants.

II. EXPERIMENTAL DETAILS AND DATA ANALYSIS

High-spin states in ^{40}K were populated through the ^{27}Al(^{19}F, αnp)^{40}K reaction with a 68 MeV ^{19}F beam. The ^{19}F beam was provided by the 15UD Pelletron accelerator at the Inter-University Accelerator Centre (IUAC), New Delhi. The 0.43 mg/cm^2 thick ^{27}Al target was evaporated on 11.4 mg/cm^2 Au backing. A multidetector array (INGA setup), comprising 12 Compton suppressed clover detectors at the time of experiment, was used to detect the γ rays. These twelve detectors were mounted at four different angles, i.e., 148° (4), 90°(4), 57°(1), and 32°(3) with respect to the beam axis. The relevant details of the experimental setup are discussed in Ref. [19]. About 10^8 twofold γ-γ coincidence events were recorded in list mode. The data sorting program, NIASMARS [20], developed at IUAC, was used to generate angle-independent symmetric and angle-dependent asymmetric γ-γ matrices, which were analyzed by INGASORT [21].

Usually, the energy calibration of the clover detectors is performed with ^{152}Eu and ^{66}Ga radioactive sources. The maximum energy emitted from the ^{152}Eu source is 1408 keV. Hence, the ^{66}Ga source, which has γ rays of energies in the range of 833 to 4806 keV, is used for high-energy calibration. Since we have transition energies more than 1.5 MeV, the ^{66}Ga source was prepared through the ^{51}V(^{19}F, 3np)^{66}Ga reaction at 68 MeV in the same experimental setup. But, ^{66}Ga was not used for energy calibration because we observed energy shifts in a few runs during the experiment. As a result, we did energy calibration of each of the files of all the runs individually using the online γ's, ranging from 300 to 4000 keV. The ^{152}Eu source was used for initial energy calibration only. The relative efficiency calibrations of the clovers were performed with ^{152}Eu and ^{66}Ga radioactive sources.

The level scheme of ^{40}K was studied based on the coincidence relationship, relative intensities, the ratio of directional correlation (R_{DCO}), the ratio of angular distribution (R_{ADO}), and the polarization asymmetry (Δ_{IPDCO}) values of γ rays. A total projection spectrum as well as typical gated spectrum are shown in Figs. 1 and 2, respectively. From PACE4 [22] calculations, the relative cross section of the ^{27}Al(^{19}F, αnp)^{40}K

channel was predicted as 11.1% of the total fusion cross section. γ rays from nuclei populated through other dominant channels of the reaction are therefore marked also in Fig. 1.

The spins and parities of most of the levels were not confirmed or assigned in ^{40}K. Therefore, in order to confirm or assign the spins and parities of the levels, the directional correlation of γ rays emitted from excited states (DCO) measurement was carried out. The DCO ratio (R_{DCO}) [23] of a γ transition (γ_1) is defined as the ratio of intensities of that γ ray ($I\gamma_1$) for two different angles in coincidence with another γ ray (γ_2) of known multipolarity. It is given by

$$R_{DCO} = \frac{I^{\gamma_1} \text{ observed at angle } \theta, \text{ gated by } \gamma_2 \text{ at } 90°}{I^{\gamma_1} \text{ observed at angle } 90°, \text{ gated by } \gamma_2 \text{ at } \theta}. \quad (1)$$

The R_{DCO} value depends on the multipolarities of these transitions (γ_1 and γ_2), and the angle between the detectors. In the present work, we measured the R_{DCO} for $\theta = 148°$. For stretched transitions of the same multipolarity, the R_{DCO} value is close to unity, and for a stretched dipole (quadrupole) transition gated by a pure quadrupole (dipole) transition, it is nearly 0.5 (2). For a mixed transition, it deviates from the mentioned values. For the assignment of the spins and the γ-ray multipole mixing ratios (δ), the experimental R_{DCO} values were compared with theoretical values calculated using the computer code ANGCOR [23]. Spin alignment parameter $\sigma/J = 0.3$, obtained from a few known $E1$ and $E2$ transitions of ^{37}Ar and ^{42}Ca, was used for this calculation.

The DCO measurement could not be carried out for a few transitions due to their low statistics. So, the angular distribution from oriented nuclei (ADO) measurement was carried out to determine their multipolarities. Two asymmetric matrices were constructed for ADO measurement. In the first matrix, the events from detectors at all angles (except 90°) are stored in the first axis and in the second axis we stored the events from the 90° detectors only. Similarly, in the second matrix, the events from detectors at all angles (except 148°) are stored in the first axis and in the second axis we stored the events from the 148° detectors only. The ADO ratio (R_{ADO}) [24] of a
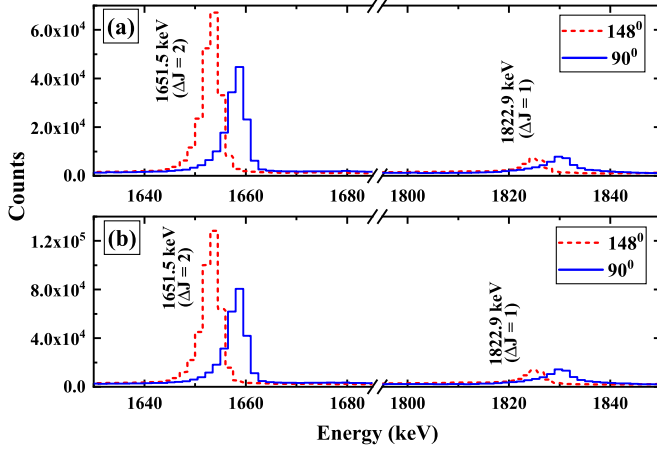
FIG. 3. A schematic representation of (a) DCO and (b) ADO spectra in ^{40}K. These spectra (a) and (b) are generated by putting gate on 891 keV ($\Delta J = 1$) transition. The 90° spectra have been artificially shifted by 5 keV for a clear view.
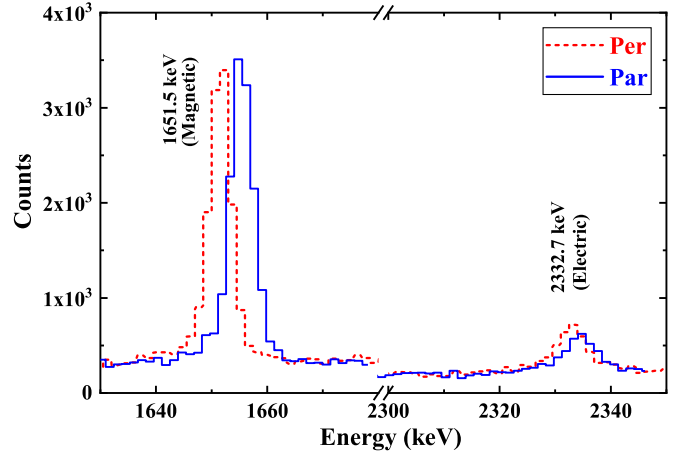

FIG. 4. Spectra generated from perpendicular and parallel matrices indicating the electric (magnetic) nature of 2332.7 keV (1651.5 keV) transition. These spectra are generated by putting gates on 891 keV. The parallel spectrum have been artificially shifted by 5 keV for a clear view.

transition is then defined as

$$R_{\text{ADO}}$$
$$= \frac{I_{\gamma_1} \text{ measured at } \theta = 148°, \text{ gated by } \gamma_2 \text{ at all angles}}{I_{\gamma_1} \text{ measured at } \theta = 90°, \text{ gated by } \gamma_2 \text{ at all angles}}. \quad (2)$$

For the present setup, R_{ADO} is 0.6 for the pure dipole transition and 1.6 for the pure quadrupole transition and the $\Delta J = 0$ transition. These values are estimated from the measured R_{ADO} values of a few known pure dipole and quadrupole transitions of ^{42}Ca [1]. In the case of mixed transitions, depending on the extent of mixing (δ), R_{ADO} may change from these values. A schematic representation of DCO and ADO spectra is shown in Fig. 3.

The integrated polarization directional correlation of oriented nuclei (IPDCO) [25] measurement was performed to assign the electric or magnetic nature of the transition. Two asymmetric matrices named parallel and perpendicular matrices were therefore constructed for IPDCO measurement. In the parallel (perpendicular) matrix, the simultaneous events detected in the two crystals of 90° clover detectors which are parallel (perpendicular) to the emission plane are recorded in the first axis, and on the second axis the coincident γ-rays detected in any other clover detector are recorded. The polarization asymmetry then expressed as

$$\Delta_{\text{IPDCO}} = \frac{a(E_\gamma)N_\perp - N_\parallel}{a(E_\gamma)N_\perp + N_\parallel}, \quad (3)$$

where $N_\perp$ and $N_\parallel$ are the intensities of full peak observed in the perpendicular and parallel matrices, respectively. The asymmetry correction factor [$a(E_\gamma)$] represents the geometrical asymmetry of the clover detectors placed at 90°. It is defined as

$$a(E_\gamma) = \frac{N_\parallel}{N_\perp}. \quad (4)$$

In the present work, ^{152}Eu and ^{66}Ga radioactive sources were used to extract the asymmetry correction factor $a(E_\gamma)$. In order to measure the Δ_{IPDCO} of the transition, we put a gate on coincident γ's on the second axis and measured the intensities of the transition of interest from the projected parallel and perpendicular spectra. A positive value of Δ_{IPDCO} implies a pure electric transition whereas a negative value indicates pure magnetic transition. For a mixed transition, the value comes close to zero and the sign depends on the amount of mixing. Figure 4 shows the spectra obtained from parallel and perpendicular matrices.

III. RESULT AND DISCUSSION

In the present work, we are not able to extend the level scheme above 8 MeV, but we have modified the existing level scheme based on the coincidence relationship, relative intensities, R_{DCO}, R_{ADO}, and Δ_{IPDCO} values of the γ transitions (Fig. 5). We have added fourteen new γ's and six new levels to the existing level scheme. The relative intensities of most of the transitions were determined from the 891 keV gated spectrum generated from the angle-independent symmetric matrix. Using proper normalization, relative intensities of the 891 keV transition and the transitions parallel to the 891 keV transition were measured from the total projection spectrum. Finally, by considering the intensity of the 891 keV transition to 100, the relative intensities of all the transitions were normalized. They are listed in Table I. We have separately measured the branching ratios of most of the levels, i.e., the gate was put on any transition above the level of interest. They are listed in Table II. In the following sections, we discuss our results in detail.

A. Levels with excitation energy ⩽4 MeV

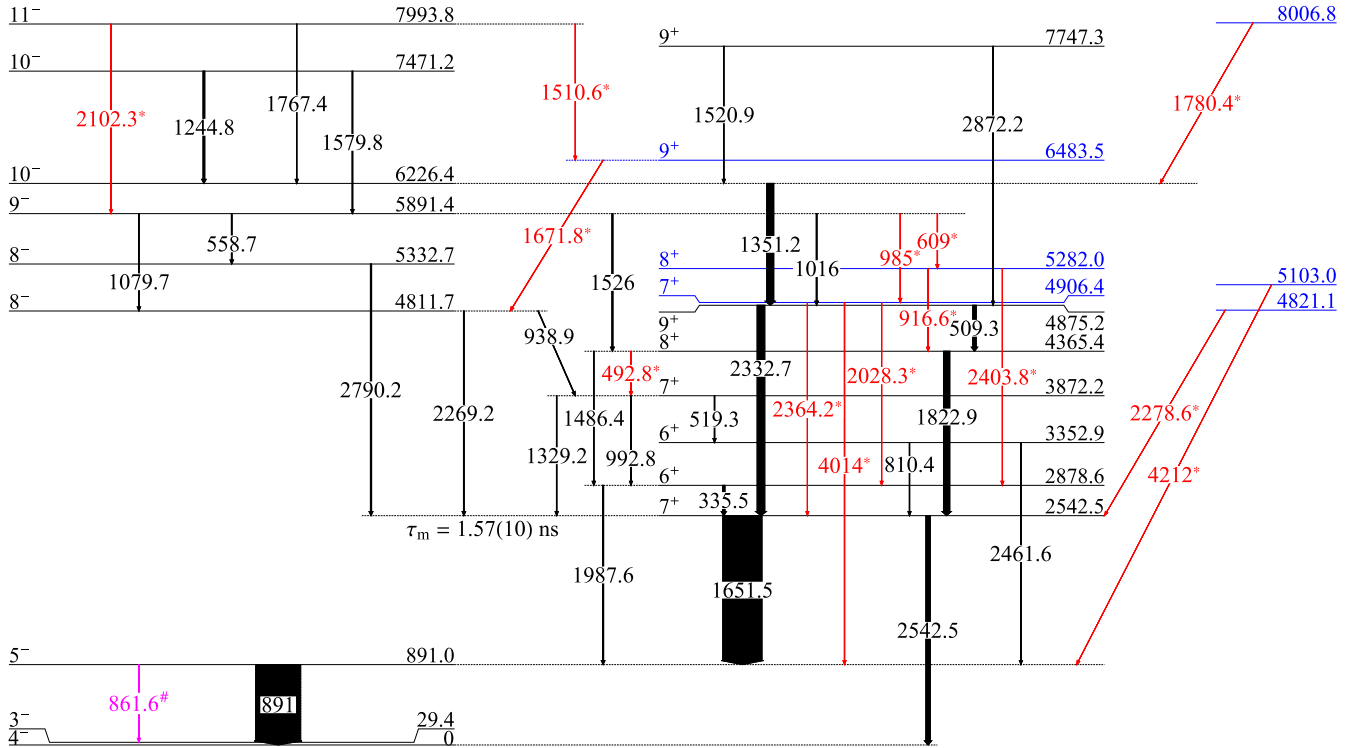We did not observe any new transitions below 4 MeV excitation energy. We have only confirmed the spin and parity of a

FIG. 5. Partial level scheme of ^{40}K. Energies are given in keV. Newly assigned γ transitions (red) and those already observed in light-ion-induced reactions (magenta) are indicated by * and #, respectively. New levels are indicated by blue lines.

few levels in this energy domain. Earlier, the spin and parity of 3352.9 and 3872.2 keV levels were assigned as (6^+) and (7^+), respectively [17]. In the present work, we measured the R_{DCO}, R_{ADO}, and Δ_{IPDCO} values of the decay out transitions from these levels to confirm their J^π assignments. The measured R_{DCO} value of the 810.4 keV transition decaying from the 3352.9 keV level is 0.89(16) and has negative Δ_{IPDCO}. The 810.4 keV is therefore a magnetic dipole transition. Hence, we have confirmed the J^π of 3352.9 keV level as 6^+. The R_{DCO} of the 2461.6 keV transition also supports this assignment. The spin and parity of the 3872.2 keV level is confirmed based on the R_{DCO}, R_{ADO}, and Δ_{IPDCO} values of 519.3, 992.8, and 1329.2 keV transitions. The measured R_{DCO} values of 519.3, 992.8, and 1329.2 keV transitions are 0.57(11), 0.96(19), and 1.35(24), respectively. The Δ_{IPDCO} of 519.3 and 1329.2 keV transitions are negative and positive, respectively. In the case of the $\Delta J = 0$ transition, the positive (negative) Δ_{IPDCO} value represents the magnetic (electric) nature of the transition [8]. Therefore, the spin and parity of the 3872.2 keV level is confirmed as 7^+.

The spins and parities of all other levels with excitation energy $\leqslant 4$ MeV were confirmed in the present work. In this energy range, we extracted the multipole mixing ratios (δ) for ten transitions and compared them with the earlier measurements [1], if available. For extracting the mixing ratios of 891 and 1651.5 keV transitions, we used R_{DCO} value of the 1486.4 keV transition gated by 891 and 1651.5 keV transitions, respectively. Most of the measured multipole mixing ratios (δ) agreed with the earlier measurements (Table I). In our present work, the sign convention proposed by Krane and Steffen is used for mixing ratio (δ) calculation [26].

The 861.6 keV transition, found in the 1651.5 keV gated spectrum, was added to the level scheme (Fig. 5). This transition was previously observed in light-ion induced experiments [1].

B. Levels with excitation energy between 4 and 6 MeV

In this energy range, four new levels (4821.1, 4906.4, 5103, and 5282 keV) and ten new transitions were added to the existing level scheme (Fig. 5). The spin and parity of 4811.7 keV level is examined based on the spectroscopic properties of 938.9 and 2269.2 keV transitions. The measured R_{DCO} and Δ_{IPDCO} values of 938.9 and 2269.2 keV transitions confirmed their electric dipole nature, which implies a modification of the parity assignment of the 4811.7 keV level from (8^+) to 8^-. The spin and parity of the 5332.7 keV level was previously assigned as (9^+) [17]. The 5332.7 keV level decays to the 2542.5 keV (7^+) level through the 2790.2 keV transition. The R_{DCO} and Δ_{IPDCO} of 2790.2 keV confirmed its electric dipole nature. We have therefore modified the spin and parity of the 5332.7 keV level from (9^+) to 8^-. The spin and parity of 4365.4, 4875.2, and 5891.4 keV levels were previously assigned as (8^+), 9^+, and (9^-), respectively. In the present work, we have confirmed the earlier assignments based on the R_{DCO}, R_{ADO}, and Δ_{IPDCO} values of the decay out transitions of these levels. In the following subsections, we discuss our new findings in detail.

1. 492.8 keV γ decay from 8_1^+ to 7_2^+ level

The 492.8 keV transition is in coincidence with 891, 1329.2, 1351.2, and also with 1651.5 keV [Fig. 6(a)].

TABLE I. Relative intensity (I_{rel}), R_{DCO}, R_{ADO}, Δ_{IPDCO}, and mixing ratio (δ) of the γ transitions in ^{40}K.

E_γ	E_X				E_{gate}				Δ_{IPDCO}	Mixing ratio (δ)	
(keV)	(keV)	I_{rel}	J_i^π	J_f^π	(keV)	ΔJ_{gate}	R_{DCO}	R_{ADO}	Expt.	Present	Previous [1]
335.5(8)	2878.6(8)	5.3(4)	6_1^+	7_1^+	891	1	0.92(9)	0.93(7)		$-0.04(7)$	$+0.01(2)$
492.8(9)	4365.4(9)	0.60(6)	8_1^+	7_2^+	891	1	0.85(16)	1.00(17)		$+0.03^{+0.10}_{-0.12}$	
509.3(7)	4875.2(7)	7.8(14)^a	9_1^+	8_1^+							
519.3(9)	3872.2(9)	1.13(7)	7_2^+	6_2^+	891	1	0.57(11)	0.55(9)	$-0.11(9)$	$-0.19^{+0.10}_{-0.13}$	
558.7(7)	5891.4(9)	1.59(10)	9_1^-	8_2^-	891	1	0.84(8)	0.88(8)	$-0.11(7)$	$+0.03(6)$	
609.0(9)	5891.4(9)	0.91(11)	9_1^-	8_2^+	891	1	0.70(13)	0.79(12)	$+0.08(7)$	$-0.08^{+0.10}_{-0.12}$	
810.4(9)	3352.9(9)	0.90(7)	6_2^+	7_1^+	891	1	0.89(16)	0.99(13)	$-0.10(8)$	$+0.06^{+0.10}_{-0.11}$	
861.6(8)	891.0(8)	0.5(1)	5_1^-	3_1^-	1651.5	2	1.1(4)	1.2(3)			E2
891.0(6)	891.0(8)	100(5)	5_1^-	4_1^-	1651.5	2	0.63(4)	0.91(5)	$-0.07(1)$	$+0.14^{+0.12}_{-0.10}$	$+0.09(2)$
916.6(7)	5282.0(8)	0.74(8)	8_2^+	8_1^+	891	1	1.42(25)	1.32(21)	$+0.14(9)$	$-0.20(37)$	
938.9(7)	4811.7(7)	1.11(9)	8_1^-	7_2^+	1329.2	0	0.59(6)	0.75(7)	$+0.13(9)$	$-0.01(6)$	
985.0(7)	5891.4(9)	1.15(13)	9_1^-	7_3^+	891	1	1.6(3)	1.56(23)	$-0.12(11)$	$+0.08^{+0.27}_{-0.24}$	
992.8(9)	3872.2(9)	0.45(4)	7_2^+	6_1^+	891	1	0.96(19)	0.93(15)		$+0.11^{+0.11}_{-0.13}$	
1016.0(7)	5891.4(9)	1.8(2)	9_1^-	9_1^+	891	1	1.46(17)	1.41(14)	$-0.06(9)$	$-0.15^{+0.35}_{-0.25}$	
1079.7(7)	5891.4(9)	1.26(9)	9_1^-	8_1^-	891	1	0.6(1)	0.71(9)	$-0.17(9)$	$-0.17^{+0.10}_{-0.13}$	
1244.8(7)	7471.2(7)	3.9(4)	10_2^-	10_1^-	1351.2	1	2.06(23)	1.67(18)	$+0.03(5)$	$-0.27^{+0.30}_{-0.34}$	$+0.13(7)$
1329.2(6)	3872.2(9)	1.08(15)	7_2^+	7_1^+	891	1	1.35(24)	1.15(19)	$+0.15(8)$	$-0.28(35)$	
1351.2(5)	6226.4(5)	15.6(9)	10_1^-	9_1^+	891	1	0.66(7)	0.76(7)	$+0.03(2)$	$-0.12(5)$	$-0.07(5)$
1486.4(6)	4365.4(9)	1.3(1)	8_1^+	6_1^+	891	1	1.53(25)	1.25(16)	$+0.04(12)$	E2	
1510.6(9)	7993.8(10)	0.45(11)	11_1^-	9_2^+	2269.2	1	1.32(22)	1.36(17)		$-0.17^{+0.18}_{-0.23}$	
1520.9(8)	7747.3(9)	0.81(13)	9_3^+	10_1^-	1351.2	1	1.00(12)	0.85(9)	$+0.09(7)$	$+0.17^{+0.18}_{-0.08}$	
1526.0(6)	5891.4(9)	2.5(3)	9_1^-	8_1^+	1822.9	1	0.83(12)	1.06(13)	$+0.13(5)$	$-0.12(9)$	
1579.8(7)	7471.2(7)	1.6(1)	10_2^-	9_1^-	2269.2	1	0.77(11)	1.07(11)	$-0.10(9)$	$-0.05(8)$	
1651.5(5)	2542.5(7)	87(5)	7_1^+	5_1^-	891	1	1.49(9)	1.6(1)	-0.06(1)	$-0.04^{+0.07}_{-0.09}$	$-0.02(3)$
1671.8(8)	6483.5(8)	0.66(7)	9_2^+	8_1^-	2269.2	1	0.86(13)	1.00(12)	$+0.17(13)$	$+0.02(10)$	
1767.4(6)	7993.8(10)	0.75(9)	11_1^-	10_1^-	1351.2	1	0.51(13)	0.42(6)	$-0.14(6)$	$-0.64(24)$	
1780.4(9)	8006.8(9)	0.17(3)									
1822.9(5)	4365.4(9)	14(1)	8_1^+	7_1^+	891	1	0.79(9)	0.87(9)	$-0.08(2)$	$-0.01(6)$	
1987.6(6)	2878.6(8)	2.2(2)	6_1^+	5_1^-	891	1	0.66(8)	0.65(7)	$+0.13(12)$	$-0.10(7)$	$-0.05(4)$
2028.3(9)	4906.4(20)	0.34(5)	7_3^+	6_1^+	891	1		1.0(4)			
2102.3(10)	7993.8(10)	0.22(3)									
2269.2(6)	4811.7(7)	1.71(12)	8_1^-	7_1^+	891	1	0.90(16)	0.63(9)	$+0.14(10)$	$+0.11(5)$	
2278.6(11)	4821.1(11)	0.12(3)									
2332.7(6)	4875.2(7)	17(1)	9_1^+	7_1^+	891	1	1.47(15)	1.32(12)	$+0.08(3)$	E2	
2364.2(9)	4906.4(20)	0.37(5)	7_3^+	7_1^+	891	1		1.7(4)			
2403.8(8)	5282.0(8)	0.27(4)	8_2^+	6_1^+	891	1		1.8(5)			
2461.6(7)	3352.9(9)	0.62(7)	6_2^+	5_1^-	891	1	0.70(19)	0.81(16)		$-0.07^{+0.14}_{-0.18}$	
2542.5(7)	2542.5(7)	9.8(7)	7_1^+	4_1^-	1351.2	1	2.8(3)	2.4(2)	$+0.07(6)$	$+0.01^{+0.36}_{-0.29}$	$+0.10(7)$
2790.2(7)	5332.7(7)	2.6(2)	8_2^-	7_1^+	891	1	0.61(9)	0.79(9)	$+0.17(10)$	$-0.16(9)$	
2872.2(9)	7747.3(9)	0.37(6)	9_3^+	9_1^+	891	1		1.4(6)			
4014(2)	4906.4(20)	0.90(8)	7_3^+	5_1^-	891	1	1.23(26)	1.41(19)	$-0.11(9)$	$-0.30^{+0.25}_{-0.40}$	
4212(2)	5103(2)	0.19(4)									

^{a}Intensity is taken from Ref. [17] with proper normalization.

According to the previous level scheme [17], 1329.2 keV was not in coincidence with 1351.2 and 1526 keV transitions. However, we observed 1351.2 and 1526 keV transitions in the 1329.2 keV gated spectrum. Hence, we have placed the 492.8 keV transition in the level scheme (Fig. 5).

2. 4906.4 keV level

The 2028.3, 2364.2, and 4014 keV transitions are in coincidence with the 985 keV transition but not in coincidence

with each other [Fig. 6(b)]. On the other hand, these four transitions are also present in the 891 keV gated spectrum (Fig. 2). The 985, 2028.3, and 2364.2 keV transitions are also in coincidence with the 1651.5 keV transition. But the 4014 keV transition is not in coincidence with 1651.5 keV transition [Fig. 6(c)]. Based on the coincidence relationship and the relative intensities, we have placed them by adding a new 4906.4 keV level in the level scheme. The spin and parity of the newly observed 4906.4 keV level is assigned as 7$^+$, based on the R_{DCO}, R_{ADO} and Δ_{IPDCO} values of 985

TABLE II. Branching ratios of different levels in ^{40}K.

E_X (keV)	E_γ (keV)	Branching ratio
891.0	861.6	0.5(1)
	891.0	99.5(1)
2542.5	1651.5	87(5)
	2542.5	13(5)
2878.6	335.5	65(4)
	1987.6	35(4)
3352.9[a]	810.4	59(5)
	2461.6	41(5)
3872.2	519.3	45.7(28)
	992.8	18.3(16)
	1329.2	36(3)
4365.4	492.8	4(1)
	1486.4	8(1)
	1822.9	88(5)
4811.7	938.9	36(6)
	2269.2	64(6)
4875.2[a]	509.3	31(6)
	2332.7	69(6)
4906.4	2028.3	19.5(16)
	2364.2	24.7(17)
	4014.0	55.8(37)
5282.0	916.6	73(8)
	2403.8	27(8)
5891.4	558.7	21.3(14)
	609.0	11.3(8)
	985.0	12.0(9)
	1016.0	17.2(12)
	1079.7	12.5(9)
	1526.0	25.7(18)
7471.2 [a]	1244.8	71(7)
	1579.8	29(7)
7747.3[a]	1520.9	69(11)
	2872.2	31(11)
7993.8[a]	1510.6	32(8)
	1767.4	53(6)
	2102.3	15(2)

[a]Estimated from relative intensities.

and 4014 keV transitions. Owing to weak statistics, we can only measure the R_{ADO} values of 2028.3 and 2364.2 keV transitions, and the measured R_{ADO}'s of these transitions also support the spin assignment of the 4906.4 keV level.

3. 5282 keV level

The 609 and 916.6 keV transitions are in coincidence with each other and also in coincidence with 891, 1651.5, and 1822.9 keV transitions [Figs. 6(d) and 6(e)]. On the other hand, the 2403.8 keV transition is present in the 609 keV gated spectrum [Fig. 6(d)], but not in the 916.6 keV gated spectrum [Fig. 6(e)]. The 2403.8 keV transition is also in coincidence with 335.5, 891, and 1651.5 keV transitions. Based on the coincidence relationship and relative intensities, we have placed the 609 keV transition above the 916.6 and 2403.8 keV transitions and added a new level at 5282 keV. The spin and
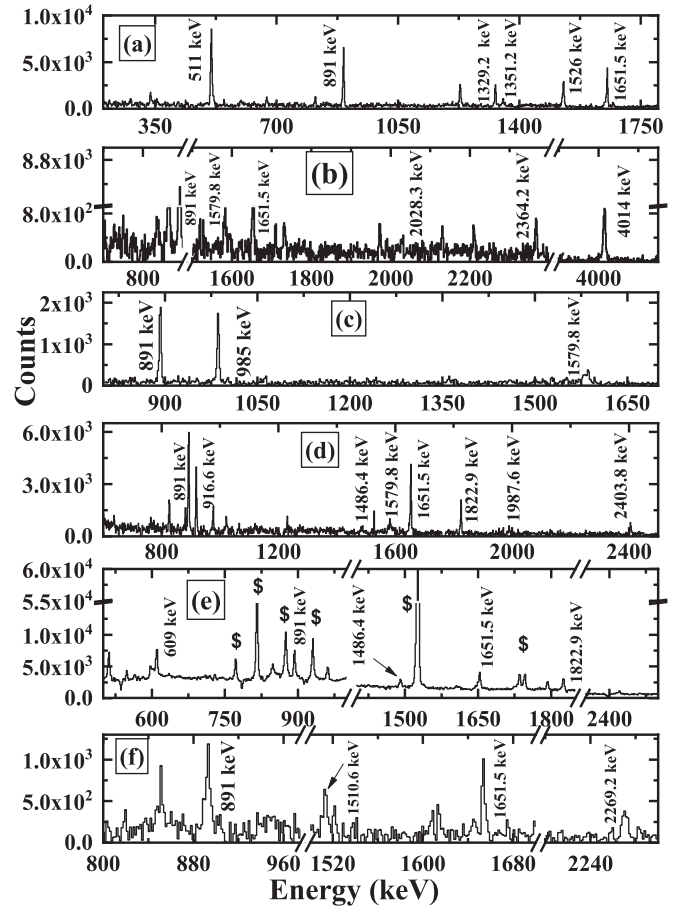

FIG. 6. Background subtracted coincidence spectra obtained by putting gates on (a) 492.8 keV, (b) 985 keV, (c) 4014 keV, (d) 609 keV, (e) 916.6 keV, and (f) 1671.8 keV transitions. In panel (e) the transitions marked with **$** are from ^{42}Ca [27].

parity of the 5282 keV level is assigned as 8^+, based on the R_{DCO}, R_{ADO} and Δ_{IPDCO} values of 916.6 keV.

4. 4821.1 and 5103 keV levels

We have added two more energy levels, 4821.1 and 5103 keV, in this energy domain. However, due to the weak statistics of the decay out 2278.6 and 4212 keV transitions, we are not able to assign their spin and parity in the present work.

In this energy domain, the mixing ratios (δ) of thirteen transitions were measured for the first time (Table I).

C. Levels with excitation energy ⩾6 MeV

In this energy domain, two new levels (6483.5 and 8006.8 keV) and three new transitions (viz. 1510.6, 1671.8, and 2102.3 keV) were added to the existing level scheme (Fig. 5).

1. 6483.5 keV level

The 1510.6 and 1671.8 keV transitions, though in coincidence with each other and also in coincidence with 891, 1651.5, and 2269.2 keV transitions, are not in coincidence

with 1822.9 and 2332.7 keV transitions [Fig. 6(f)]. The relative intensity of the 1671.8 keV transition is greater than that of 1510.6 keV. We have therefore placed 1510.6 keV above the 1671.8 keV transition and added a new level at 6483.5 keV. The spin and parity of the 6483.5 keV level is assigned based on the R_{DCO}, R_{ADO} and Δ_{IPDCO} values of the 1671.8 keV transition (Table I).

2. 1780.4 and 2102.3 keV transitions

In our present study, we have identified the 2102.3 keV transition, which is in coincidence with 558.7, 891, 1651.5, and 2790.2 keV transitions. So, we have placed 2102.3 keV as the decay out transition from the 7993.8 keV level in the current level scheme. A new 1780.4 keV transition decaying from the 8006.8 keV level is observed in the present work. But, due to poor statistics of the 1780.4 keV transition, we could not assign the spin and parity of the 8006.8 keV level.

We have confirmed the spin and parity of the 6226.4 keV level as 10^-. It was earlier assigned as (10^-) [17]. Soderstrom *et al.* [17] reported three new levels, viz., 7471.2, 7747.3, and 7993.8 keV, in their level scheme. But they did not assign the spin and parity of these levels. In the present work, we have assigned the spin and parity of these levels based on the R_{DCO}, R_{ADO} and Δ_{IPDCO} values of the decay out transitions. The 7471.2 keV level decays to the 5891.4 keV level (9^-) through the 1579.8 keV magnetic dipole transition (Table I). We have therefore assigned 10^- as the spin and parity of 7471.2 keV level. The R_{DCO} and Δ_{IPDCO} values of 1244.8 keV transition also support the present assignment. In a similar way, we have assigned the spin and parity of 7747.3 and 7993.8 keV levels using the R_{DCO} and Δ_{IPDCO} values of 1520.9 and 1767.4 keV transitions, respectively. In this energy domain, the mixing ratios (δ) of five transitions were measured for the first time (Table I).

The 7033 keV level was placed in the previous level scheme [17]. It decays to the 4812 keV level through the 2220 keV transition. A weak 1142 keV transition was also tentatively assigned between 7033 and 5892 keV levels. In the present work, we could not observe 1142 and 2220 keV decay out transitions from the 7033 keV level (Fig. 7). We therefore removed the 7033 keV level from our present level scheme (Fig. 5).

In the present work, uncertainties quoted in the measured values of intensities, R_{DCO}, and R_{ADO} are due to the statistical errors and the errors from the detector efficiency. The uncertainties quoted in the γ energy are extracted from peak fitting and detector calibration errors. Since we did not consider efficiency corrections for polarization measurements, the uncertainties quoted in the Δ_{IPDCO} measurements are statistical only.

In the following section, we compare our experimental observation with the shell-model results.

IV. THEORETICAL CALCULATION

Large-basis shell-model calculations were performed using the code OXBASH [28] to understand the microscopic origin of each excited state in ^{40}K. The valence space consists of $1d_{5/2}$,
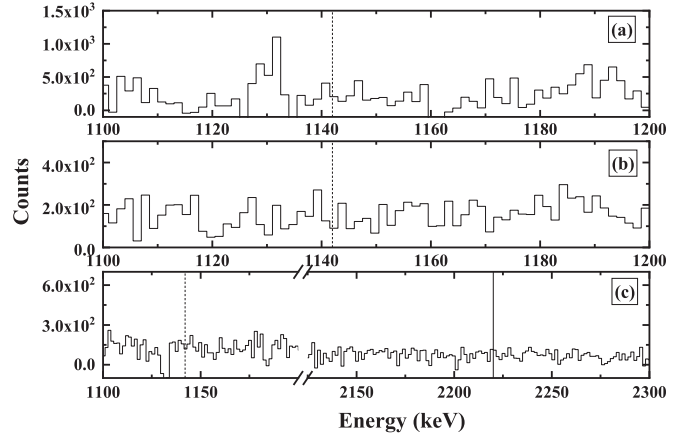

FIG. 7. Background subtracted coincidence spectra obtained by putting gates on (a) 558.7 keV, (b) 2269.2 keV, and (c) 2790.2 keV transitions. The position of 1142 keV transition in panels (a)–(c) is marked by a dotted line. The position for the 2220 keV transition in (c) is marked by a solid line.

$1d_{3/2}$, $2s_{1/2}$, $1f_{7/2}$, $1f_{5/2}$, $2p_{3/2}$, and $2p_{1/2}$ orbitals for both protons and neutrons above the ^{16}O inert core. The number of valence particles (protons + neutrons) in ^{40}K is 24. The sdpfmw interaction [29] (as referred to within the OXBASH [28] code package) was used for the calculation. Other relevant details of the interaction and calculation are discussed in Ref. [3].

Unrestricted calculations for ^{40}K with such a large number of valence particles in the full sd-pf space are not possible due to the large m-scheme basis dimension. Therefore, several particle restrictions in the model space were used in our calculations. During our calculations, we observed that the calculated energies are overpredicted for the positive parity and high spin negative parity states. In these calculations, multiparticle multihole excitations between sd and pf shells are involved. Therefore, we changed the single-particle energy (SPE) of each of the pf orbitals by 600 keV to improve the calculated energies. The results for energy spectra and transition probabilities in ^{40}K with different particle restrictions are discussed in the next sections. For all these calculations, the mass normalization factor, defined as the number of particles up to the sd shell, was taken accordingly.

A. Negative parity states

We adopted two different truncation schemes (Theor-N1 and Theor-N2) for the negative parity states.

1. Theor-N1

The particle partition of Theor-N1 is $(sd)^{-1}$-$(pf)^1$. In case of ^{40}K, the maximum possible spin which can be generated in this particle configuration is 5^-. We therefore calculated the excitation energies for 3^-, 4^-, and 5^- levels and compared them with the experimental energies. The comparison shows a very good agreement with experimental values (Fig. 8). In the calculation, the full sd-pf shell was used and the mass normalization factor was 39.

11^-	7993.8			
10^-	7471.2	10^-	7621	
		11^-	7278	
10^-	6226.4	8^-	6275	
		10^-	6023	
9^-	5891.4	9^-	5943	
8^-	5332.7	8^-	5399	
8^-	4811.7			
5^-	891	5^-	891.0	
3^-	36	3^-	29.4	4^- 0
4^-	0	4^-	0	
Theor−N1		Expt		Theor−N2

FIG. 8. Comparison of theoretical and experimental level schemes for negative parity states in ^{40}K. All these energies are plotted with respect to the ground state energy (-272.871 MeV) as 0.

2. Theor-N2

We excited two particles [$(sd)^{-3}$-$(pf)^3$ excitation] to the pf orbitals to generate the high spin negative parity states (Theor-N2) of ^{40}K. In the calculation, the full sd-pf shell was used and the mass normalization factor was 37. The results (Fig. 8) show that the calculated energies of 9^-_1, 10^-_1, and 10^-_2 levels agree reasonably well with the experimental energies. However, the 8^-_1 and 8^-_2 states are overpredicted by 587 and 942 keV, respectively. Interestingly, the calculated energy of the 8^-_1 level (5399 keV) is very close to the experimental energy of the 8^-_2 level (5332.7 keV). Since we performed our calculation with a particular configuration i.e. 1p-1h, or 2p-2h, or 3p-3h, etc., the deviation between the experimental and the calculated energy obtained from the shell model may be due to the mixing of different mp-mh configurations. Therefore, both
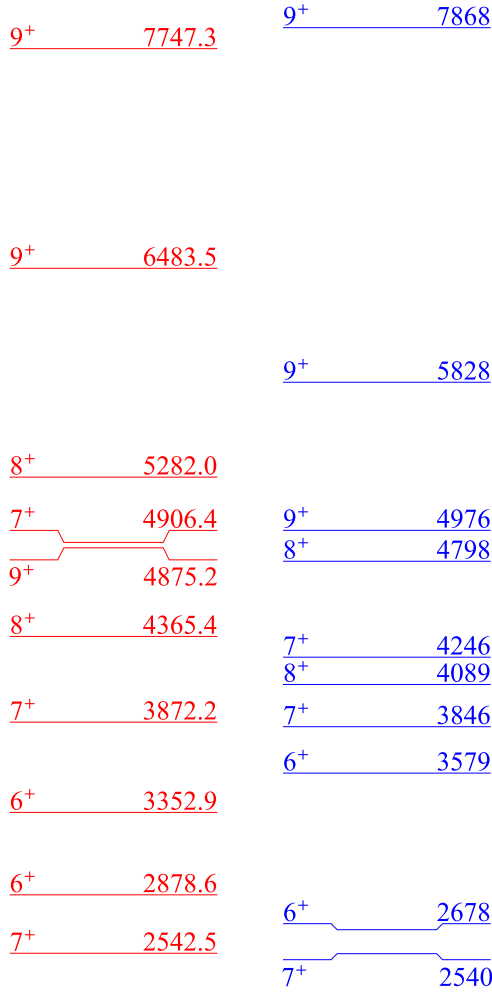
4811.7 and 5332.7 keV levels are either mixed levels (3p-3h + 5p-5h configuration) or the 5332.7 keV level is generated from pure 3p-3h excitation and only the 4811.7 keV level is a mixed state. Since the full sd-pf model space calculation for 5p-5h excitation is not possible with the present computational facility, the microscopic origins of 4811.7 and 5332.7 keV levels are not confirmed in the present work. It was also noticed that the 11^-_1 state is underpredicted by 716 keV (Fig. 8).

B. Positive parity states

We used one truncation scheme named Theor-P1 to reproduce the positive parity states in ^{40}K. In Theor-P1, only one particle is excited (2h-2p) to the pf shell, and the full sd-pf model space was used to generate the positive parity states. The particle configuration for the truncation is therefore $(sd)^{-2}$-$(pf)^2$. The comparison between experimental and calculated energies is shown in Fig. 9. The figure shows that, except for 7^+_3 and 9^+_2 levels, the experimental and theoretical energies are agreed well. For 7^+_3 (4906.4 keV) and 9^+_2 (6483.5 keV) levels, the calculated energies are underpredicted by $\approx$650 keV. The mass normalization factor for sd shell two-body matrix elements (TBMEs) for this calculation was 38.

C. Configuration mixing and Collectivity

The decompositions of the wave functions for the positive and negative parity states in ^{40}K are shown in Tables III and IV, respectively. We used the results obtained from Theor-N1 truncation for the low-lying negative parity states. Similarly, for the high spin positive and negative parity states, Theor-P1 and Theor-N2 truncations were used, respectively. The probability and the structure of different partitions having >10% contribution are shown in the tables (Tables III and IV). The partitions are given in terms of occupation numbers of single-particle valence orbits. Here, N_1 is the total number of particle partitions for a particular state, each with contribution >1%, and N_2 gives an estimation of the minimum number of particle partitions, each of which contributes $\leqslant$1% in the state.

Table III shows that the positive-parity states are primarily generated from single-particle excitations. They have a much smaller extent of configuration mixing. For the positive parity states (6^+–9^+), the largest particle partition in their wave function is 67%–93%. Low-lying negative parity states with $(sd)^{-1}$-$(pf)^1$ configuration have 1–3 particle partitions with the largest 99% (Table IV). However, the configuration mixing in terms of single-particle partitions for the high spin negative parity states (8^-–11^-) was increased. It was found that they have 9–12 particle partitions contributing at least 1% with the largest 44%–69% in their wave function. These high spin negative parity states therefore show a considerable amount of configuration mixing in terms of particle partitions. Consequently, these give us a sign of collective excitations at higher excitation energy in ^{40}K.

The reduced transition probabilities [$B(E1)$, $B(M1)$, $B(E2)$, $B(M2)$, and $B(E3)$] for a few transitions were calculated by using the effective charges $e_p = 1.5e$ and $e_n = 0.5e$ and free values of g factors [4,6,7,30–32]. The experimental transition strengths were extracted from the reported level

FIG. 9. Comparison of theoretical and experimental level schemes for positive parity states in ^{40}K. All these energies are plotted considering the ground state energy (-272.871 MeV) as 0.

lifetimes [1]. The branching and mixing ratios are taken from the present measurement. The calculated $B(E2)$, $B(M2)$, and $B(E3)$ values show good agreement with the corresponding available experimental data (Table V). The calculated and experimental $B(E1)$ and $B(M1)$ values vary slightly but are

TABLE III. Structure of the wave functions for the positive parity states in ^{40}K. The partitions are given in terms of occupation numbers of single-particle valence orbits in the following order : $1d_{5/2}$, $1d_{3/2}$, $2s_{1/2}$, $1f_{7/2}$, $1f_{5/2}$, $2p_{3/2}$, and $2p_{1/2}$.

		Energy (MeV)		Wave function			
J_i^π	T	Expt.	Theor.	%	Partition	N_1	N_2
7_1^+	1	2.543	2.540	88	[12,6,4,2,0,0,0]	6	3
6_1^+	1	2.879	2.678	83	[12,6,4,2,0,0,0]	7	3
6_2^+	1	3.353	3.579	69	[12,6,4,2,0,0,0]	7	4
7_2^+	1	3.872	3.846	81	[12,6,4,2,0,0,0]	5	5
8_1^+	1	4.365	4.089	89	[12,6,4,2,0,0,0]	3	3
9_1^+	1	4.875	4.976	93	[12,6,4,2,0,0,0]	3	2
7_3^+	1	4.906	4.246	67	[12,6,4,2,0,0,0]	7	3
				11	[12,7,3,2,0,0,0]		
8_2^+	1	5.282	4.798	79	[12,6,4,2,0,0,0]	7	2
				11	[12,7,3,2,0,0,0]		
9_2^+	1	6.484	5.828	91	[12,6,4,2,0,0,0]	3	1
9_3^+	1	7.747	7.868	88	[12,7,3,2,0,0,0]	4	2

of the same order of magnitude. These calculations provide evidence of the reliability of the calculated wave functions.

In the present experiment, we used a thick ^{27}Al target with Au backing to populate ^{40}K. We calculated the stopping time [33] of ^{40}K in the ^{27}Al and Au backing using the calculated range and the stopping power of ^{40}K in the target and backing medium [34]. The energy distribution of the recoils (^{40}K) was taken from PACE4 calculation [22]. The estimated stopping time of ^{40}K in the ^{27}Al and Au backing is ≈ 360 fs. So, we may observe the lineshape of the decay out transitions if the lifetimes of the levels are of the order of the estimated stopping time of ^{40}K. We have not found any lineshape of the decay out transitions in the present experiment. It was also noticed that the reported lifetimes of 2878.6 and 4365.4 keV levels are 0.39(14) and 0.52(20) ps, respectively, which are close to the estimated stopping time of ^{40}K. The calculated lifetimes of a few levels (Table V) are also of the order of the estimated stopping time. However, we have not observed any

TABLE IV. Structure of the wave functions for the negative parity states in ^{40}K. The partitions are given in terms of occupation numbers of single-particle valence orbits in the following order: $1d_{5/2}$, $1d_{3/2}$, $2s_{1/2}$, $1f_{7/2}$, $1f_{5/2}$, $2p_{3/2}$ and $2p_{1/2}$.

		Energy (MeV)		Wave function			
J_i^π	T	Expt.	Theor.	%	Partition	N_1	N_2
4_1^-	1	0	0 (-272.871)	99	[12,7,4,1,0,0,0]	2	1
3_1^-	1	0.029	0.036	96	[12,7,4,1,0,0,0]	3	1
5_1^-	1	0.891	0.891	99	[12,7,4,1,0,0,0]	1	2
8_1^-	1	4.812	5.399	54	[12,5,4,3,0,0,0]	11	9
				16	[12,5,4,2,0,1,0]		
8_2^-	1	5.333	6.275	54	[12,5,4,3,0,0,0]	11	9
9_1^-	1	5.891	5.943	60	[12,5,4,3,0,0,0]	10	7
10_1^-	1	6.226	6.023	64	[12,5,4,3,0,0,0]	10	4
10_2^-	1	7.471	7.621	44	[12,5,4,3,0,0,0]	12	7
				20	[12,5,4,2,0,1,0]		
11_1^-	1	7.994	7.278	69	[12,5,4,3,0,0,0]	9	5

TABLE V. Comparison of experimental and theoretical lifetimes and reduced transition probabilities for different transitions in ^{40}K.

E_X	τ_{mean} (ps)		J_i^π	E_γ	J_f^π	$B(E1)$ ($\times10^{-6}\,e^2$fm^2)		$B(M1)$ ($\times10^{-3}\,\mu_N^2$)		$B(E2)$ (e^2fm^4)		$B(M2)$ (μ_N^2fm^2)		$B(E3)$ (e^2fm^6)	
(keV)	Reported [1]	Theor.		(keV)		Expt.	Theor.	Expt.	Theor.	Expt.	Theor.	Expt.	Theor.	Expt.	Theor.
891.0	1.20(26)	2.3	5_1^-	861.6	3_1^-					$7.1^{+3.8}_{-2.4}$	5.5				
				891.0	4_1^-			65^{+20}_{-14}	34.9						
2542.5	1.57(10) ns	0.72 ns	7_1^+	1651.5	5_1^-										
				2542.5	4_1^-							$3.30^{+0.43}_{-0.42}$	7.96	209^{+77}_{-103}	168
2878.6	0.39(14)	0.24	6_1^+	335.5	7_1^+			2498^{+1642}_{-791}	1204						
				1987.6	5_1^-	71^{+53}_{-25}	264								
3352.9		0.34	6_2^+	810.4	7_1^+				47						
				2461.6	5_1^-		107								
3872.2		0.08	7_2^+	519.3	6_2^+				18.5						
				992.8	6_1^+				12.8						
				1329.2	7_1^+				308						
4365.4	0.52(20)	1.42	8_1^+	492.8	7_2^+			36^{+37}_{-17}	102						
				1486.4	6_1^+					17^{+14}_{-6}	17				
				1822.9	7_1^+			16^{+11}_{-5}	3.2						
4811.7		12.1	8_1^-	938.9	7_2^+		2.00								
				2269.2	7_1^+		4.3								
4875.2	<1.01	0.38	9_1^+	509.3	8_1^+				381						
				2332.7	7_1^+					>8	24.2				
4906.4		0.54	7_3^+	2028.3	6_1^+				11.7						
				2364.2	7_1^+				0.27						
				4014.0	5_1^-								4.7		
5282.0		0.30	8_2^+	916.6	8_1^+				226						
				2403.8	6_1^+						2.34				
5332.7		0.32	8_2^-	2790.2	7_1^+		89								
5891.4		0.59	9_1^-	558.7	8_2^-				226						
				609.0	8_2^+		3								
				985.0	7_3^+								0.25		
				1016.0	9_1^+		14.8								
				1079.7	8_1^-				35.5						
				1526.0	8_1^+		32.5								
6226.4		2.43	10_1^-	1351.2	9_1^+		104								
6483.5		29.7	9_2^+	1671.8	8_1^-		4.5								
7471.2		0.10	10_2^-	1244.8	10_1^-				0.60						
				1579.8	9_1^-				141						
7747.3		0.10	9_3^+	1520.9	10_1^-		31								
				2872.2	9_1^+				24.5						
7993.8		0.16	11_1^-	1510.6	9_2^+								1.06		
				1767.4	10_1^-				40.2						
				2102.3	9_1^-						43.7				

lineshape of the transitions decaying from the levels below 6.5 MeV. This may be due to the presence of long lived states at higher excitation energy, as suggested by the results obtained from shell-model calculations. For the levels above 6.5 MeV, the predicted lifetimes are in the range of 100–160 fs, and they may have lineshapes. But, we could not identify them because of their poor statistics.

D. Two-nucleon transfer spectroscopic factor calculation

It was reported in Ref. [17] that (6_2^+), (7_2^+), (8_1^+), and (9_2^+) levels possess largely the structure of a $T = 0$ and $J = 3$ multiplet coupled to the 6^+ state in ^{42}Ca. On the other hand 6_1^+, 7_1^+, (8_2^+), and 9_1^+ levels possess largely the structure of a $J = 2$ multiplet coupled to the 7^+ state in ^{42}Sc. They predicted

these based on their weak-coupling calculations. The yrast 6^+ level of ^{42}Ca is dominated by $\pi(sd)^{12}(fp)^0 \otimes \nu(sd)^{12}(fp)^2$ configuration [27,35]. The particle configuration for the yrast 7^+ level of ^{42}Sc is $\pi(sd)^{12}(fp)^1 \otimes \nu(sd)^{12}(fp)^1$ [36].

The positive parity levels of interest in ^{40}K were generated by exciting one nucleon from sd orbitals to the fp orbitals. In order to investigate the particle configuration in terms of protons and neutrons, LBSM calculations were carried out with SDPFMWPN interaction [29] for the positive parity levels in ^{40}K. The average numbers of protons and neutrons in the sd and pf orbitals for each positive parity level are shown in Table VI. ^{40}K is two nucleons away from ^{42}Ca (^{42}Ca + 1 proton hole +1 neutron hole) and ^{42}Sc (^{42}Sc + 2 proton holes). The results show that for the (6_1^+), (6_2^+), (7_2^+), (7_3^+),

TABLE VI. Average particle occupancies of positive-parity states in ^{40}K.

J^π	E_X (MeV)	$\pi 1d_{5/2}$	$\pi 1d_{3/2}$	$\pi 2s_{1/2}$	$\pi 1f_{7/2}$	$\pi 1f_{5/2}$	$\pi 2p_{3/2}$	$\pi 2p_{1/2}$	$\nu 1d_{5/2}$	$\nu 1d_{3/2}$	$\nu 2s_{1/2}$	$\nu 1f_{7/2}$	$\nu 1f_{5/2}$	$\nu 2p_{3/2}$	$\nu 2p_{1/2}$
7_1^+	2.543	5.9399	2.2015	1.9361	0.9113	0.0094	0.0015	0.0003	5.9874	3.9376	1.9975	1.0449	0.0166	0.0158	0.0002
6_1^+	2.879	5.9408	2.5958	1.9281	0.5174	0.0147	0.0027	0.0005	5.9585	3.5948	1.9820	1.4218	0.0330	0.0089	0.0011
6_2^+	3.353	5.9321	2.6201	1.9485	0.4405	0.0382	0.0160	0.0046	5.9599	3.5781	1.9612	1.3788	0.0517	0.0634	0.0069
7_2^+	3.872	5.9319	2.7371	1.9427	0.3626	0.0226	0.0016	0.0015	5.9680	3.4305	1.9897	1.5304	0.0298	0.0479	0.0036
8_1^+	4.365	5.9386	2.6356	1.9901	0.4117	0.0238	0.0001	0.0001	5.9663	3.4707	1.9987	1.5267	0.0316	0.0060	0.0001
9_1^+	4.875	5.9501	2.2030	1.9661	0.8361	0.0146	0.0001	0.0000	5.9776	3.8732	1.9999	1.1299	0.0193	0.0001	0.0000
7_3^+	4.906	5.9375	2.6704	1.8794	0.4795	0.0278	0.0032	0.0021	5.9609	3.5837	1.9680	1.3364	0.0447	0.1042	0.0021
8_2^+	5.282	5.9458	2.2717	1.8834	0.8813	0.0166	0.0004	0.0008	5.9814	3.9188	1.9989	1.0623	0.0231	0.0150	0.0006
9_2^+	6.484	5.9395	2.8836	1.9994	0.1565	0.0210	0.0001	0.0000	5.9570	3.2206	2.0000	1.7990	0.0232	0.0003	0.0000
9_3^+	7.747	5.9074	3.0730	1.0471	0.9612	0.0100	0.0013	0.0000	5.9767	3.9968	1.9991	1.0053	0.0185	0.0036	0.0000

(8_2^+), and (9_2^+) levels in ^{40}K the average number of neutrons (protons) in the fp shell is close to 2 (0) and the average number of neutrons (protons) in the sd shell is close to 11 (11). Therefore, the structure of these positive parity levels in ^{40}K can be well described by coupling one proton and one neutron hole to the sd shell of ^{42}Ca. On the other hand, for the (7_1^+), (8_2^+), (9_1^+), and (9_3^+) levels, the average number of neutrons (protons) in the fp shell is close to 1 (1) and the average number of neutrons (protons) in the sd shell is close to 12 (10). Therefore, the structure of these positive parity levels in ^{40}K can be well described by coupling two proton holes to the sd shell of ^{42}Sc. We therefore calculated the two-nucleon transfer spectroscopic factor for the positive parity states of interest in ^{40}K in terms of one proton hole + one neutron hole and two proton holes coupled to the sd shell of the low-lying positive parity states in ^{42}Ca and ^{42}Sc, respectively. The details of these calculations are discussed in the next section.

In order to perform the two-nucleon transfer spectroscopic factors calculation to obtain the parentage of the positive parity levels (6^+ to 9^+) in ^{40}K, we have to first calculate the wave function of the states of interest in ^{40}K, ^{42}Ca, and ^{42}Sc. The LBSM calculations were therefore carried out using the code OXBASH to obtain the wave function of states of interest in ^{42}Ca and ^{42}Sc. The SDPFMW effective interaction was used in these calculations. Comparisons between experimental and calculated energies of the levels in ^{42}Ca and ^{42}Sc are shown in Figs. 10 and 11, respectively.

In two-nucleon transfer spectroscopic factor calculations, for a particular state in ^{40}K, the number of contributions from different orbitals for different ΔJ (depending on the core angular momentum and the angular momentum of the level of interest) increases considerably. Therefore, we considered only the contributions having spectroscopic amplitude $\geqslant 0.05$. Whenever the maximum contribution is $\leqslant 0.05$, we took only the maximum spectroscopic amplitude. The calculated spectroscopic factors, i.e., the square of the spectroscopic amplitude, for the positive parity levels in ^{40}K are shown in Figs. 12 and 13.

The result shows that, among all the positive-parity levels in ^{40}K, 7_1^+, 8_2^+, 9_1^+, and 9_3^+ levels are primarily generated from the yrast 7^+ level of ^{42}Sc. The 6_1^+ level in ^{40}K is primarily generated from the 6^+ ($T = 1$) level of ^{42}Ca or ^{42}Sc. In

the previous work [17], 6_1^+, 7_1^+, (8_2^+), and 9_1^+ levels were identified as coupling of a pair of proton holes with $J = 2$ to the 7^+ state in ^{42}Sc. We found that the 7_3^+, 8_1^+, and 9_2^+ levels are primarily generated from the 6^+ ($T = 1$) level of ^{42}Ca or ^{42}Sc. In a similar way, 6_2^+ and 7_2^+ levels in ^{40}K are primarily generated from the 4^+ ($T = 1$) level of ^{42}Ca or ^{42}Sc. Previously, (6_2^+), (7_2^+), (8_1^+), and (9_2^+) levels were identified as the $T = 0$ and $J = 3$ multiplet coupled to the 6^+ state in ^{42}Ca [17].

FIG. 10. Comparison of theoretical and experimental positive parity levels in ^{42}Ca. Only the levels of interest are shown in this figure.

$^{42}_{21}$Sc
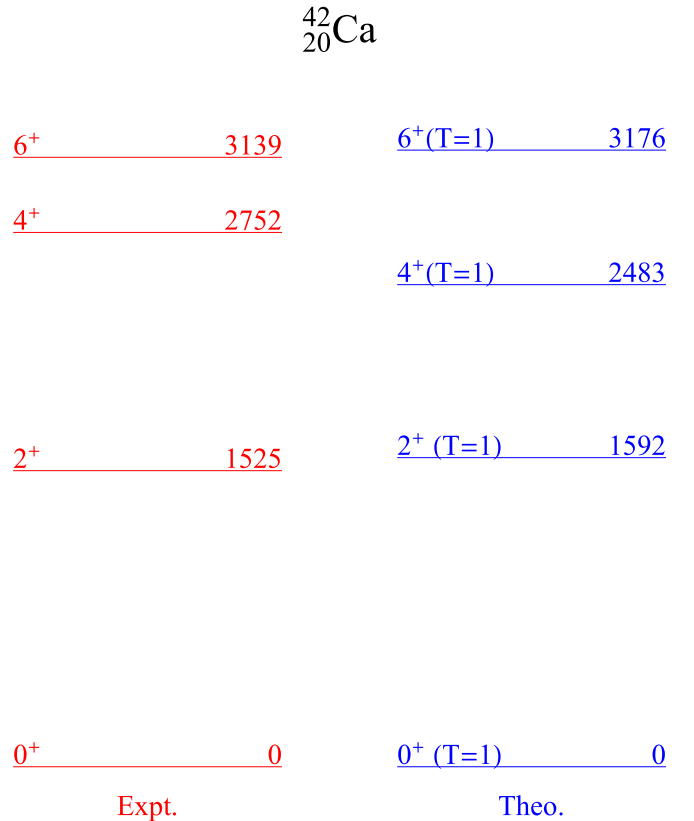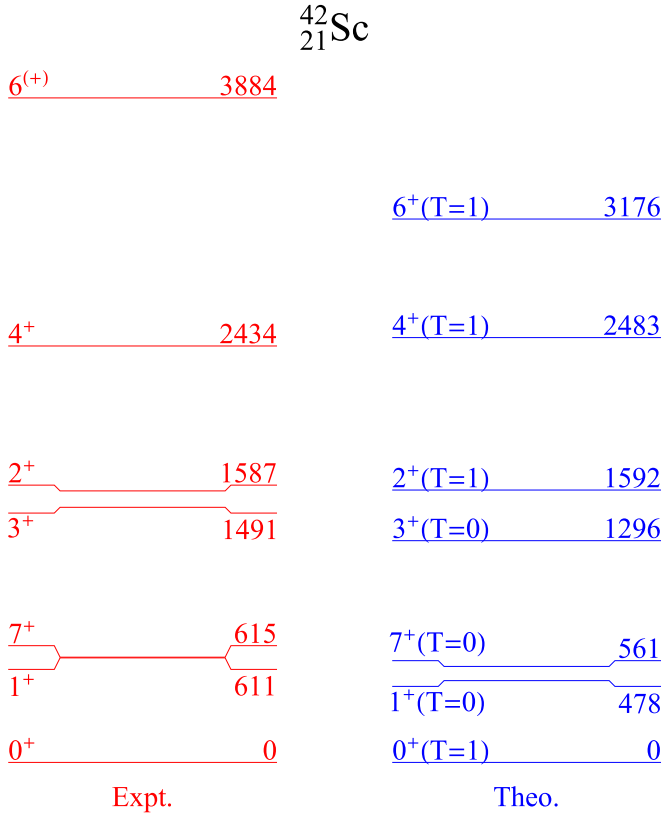
FIG. 11. Comparison of theoretical and experimental positive parity levels in ^{42}Sc. Only the levels of interest are shown in this figure.

V. CONCLUSION

High spin states of ^{40}K populated through the ^{27}Al(^{19}F, αnp)^{40}K reaction with a 68 MeV ^{19}F beam were studied using the Indian National Gamma Array (INGA) facility. Six new levels and fourteen new transitions were
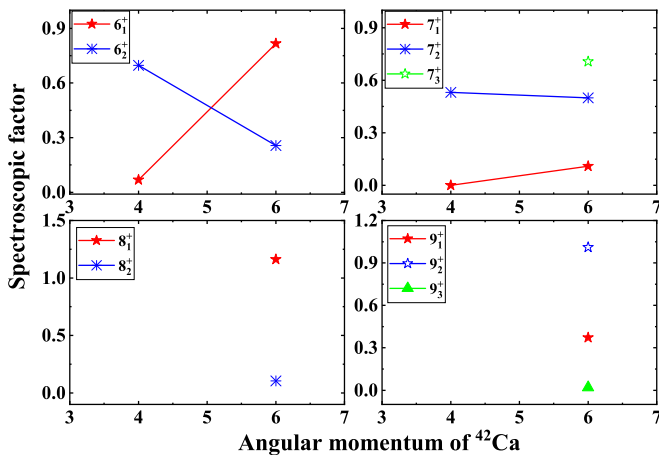

FIG. 12. Calculated spectroscopic factors for the positive-parity states in ^{40}K to estimate the contribution of the low-lying positive-parity states of the core nucleus, ^{42}Ca.
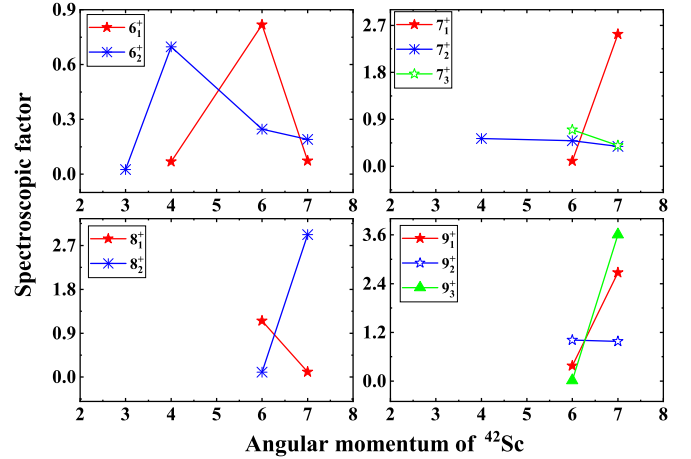
FIG. 13. Calculated spectroscopic factors for the positive-parity states in ^{40}K to estimate the contribution of the low-lying positive-parity states of the core nucleus, ^{42}Sc.

added in the existing level scheme. The spins and parities of most the levels were assigned, modified, or confirmed from R_{DCO} and linear polarization measurements. For a few weak transitions, R_{ADO} measurements were carried out to assign their dipole or quadrupole nature. The multipole mixing ratios (δ) of most of the transitions were measured. Large-basis shell-model calculations were performed to understand the microscopic origin of these levels. In our calculations, different particle restrictions in sd and pf shell orbitals were used to reproduce the experimental level scheme. Collectivity in terms of particle partitions with angular momentum and excitation energy was studied. The experimental transition strengths for a few transitions were compared with the calculated values. Level lifetimes for most of the levels were predicted based on the results obtained from LBSM calculations. Two-nucleon transfer spectroscopic factors were calculated to understand the origin of the low-lying positive parity levels in ^{40}K.

[1] http://www.nndc.bnl.gov/ensdf/.

[2] F. D. Vedova *et al.*, Phys. Rev. C **75**, 034317 (2007).

[3] R. Kshetri *et al.*, Nucl. Phys. A **781**, 277 (2007).

[4] S. Aydin *et al.*, Phys. Rev. C **86**, 024320 (2012); **89**, 014310 (2014).

[5] A. Bisoi *et al.*, Phys. Rev. C **90**, 024328 (2014).

[6] A. Bisoi *et al.*, Phys. Rev. C **89**, 024303 (2014).

[7] A. Bisoi *et al.*, Phys. Rev. C **88**, 034303 (2013).

[8] A. Das *et al.*, Phys. Rev. C **101**, 044310 (2020).

[9] R. Rahaman *et al.*, Phys. Rev. C **102**, 024315 (2020).

[10] W. J. Gerace and A. M. Green, Nucl. Phys. A **123**, 241 (1969).

[11] E. Ideguchi *et al.*, Phys. Rev. Lett. **87**, 222501 (2001).

[12] K. Hadynska-Klek *et al.*, Phys. Rev. Lett. **117**, 062501 (2016).

[13] C. E. Svensson *et al.*, Phys. Rev. Lett. **85**, 2693 (2000).

[14] D. Rudolph *et al.*, Phys. Rev. C **65**, 034305 (2002).

[15] E. Ideguchi *et al.*, Phys. Lett. B **686**, 18 (2010).

[16] Y.-C. Yang, Y.-X. Liu, Y. Sun, and M. Guidry, Eur. Phys. J. A **54**, 217 (2018).

[17] P.-A. Söderström *et al.*, Phys. Rev. C **86**, 054320 (2012).

[18] R. Rahaman *et al.*, Proc. DAE-BRNS Symp. Nucl. Phys. (India) **66**, 124 (2022).

[19] S. Muralithar *et al.*, Nucl. Instrum. Methods Phys. Res., Sect. A **622**, 281 (2010); S. Ray *et al.*, Proc. DAE-BRNS International Symp. Nucl. Phys. (India) **54**, 56 (2009).

[20] M. Jain, E. T. Subramanian, and S. Chatterjee, Rev. Sci. Instrum. **94**, 013304 (2023).

[21] R. Bhowmick *et al.*, Proc. DAE-BRNS Symp. Nucl. Phys. (India) B **44**, 422 (2001).

[22] A. Gavron, Phys. Rev. C **21**, 230 (1980).

[23] E. S. Macias, W. D. Ruhter, D. C. Camp, and R. G. Lanier, Comput. Phys. Commun. **11**, 75 (1976).

[24] M. Piiparinen, A. Ataç, J. Blomqvist, G. B. Hagemann, B. Herskind, R. Julin, S. Juutinen, A. Lampinen, J. Nyberg, G. Sletten, P. Tikkanen, S. Tormanen, A. Virtanen, and R. Wyss, Nucl. Phys. A **605**, 191 (1996).

[25] K. Starosta *et al.*, Nucl. Instrum. Methods Phys. Res., Sect. A **423**, 16 (1999).

[26] K. S. Krane and R. M. Steffen, Phys. Rev. C **2**, 724 (1970).

[27] M. Lach *et al.*, Eur. Phys. J. A **16**, 309 (2003).

[28] B. A. Brown, A. Etchegoyen, W. D. M. Rae, and N. S. Godwin, MSU-NSCL Report No. 524, 1985 (unpublished).

[29] E. K. Warburton, J. A. Becker, and B. A. Brown, Phys. Rev. C **41**, 1147 (1990).

[30] P. Mason *et al.*, Phys. Rev. C **71**, 014316 (2005).

[31] M. Ionescu-Bujor *et al.*, Phys. Rev. C **73**, 024310 (2006).

[32] M. Ionescu-Bujor *et al.*, Phys. Rev. C **80**, 034314 (2009).

[33] G. F. Knoll, *Radiation Detection and Measurement* (John Wiley and Sons, New York, 1979).

[34] J. F. Ziegler, J. Biersack, and U. Littmark, *The Stopping and Range of Ions in Matter* (Pergamon, Oxford, 1985).

[35] E. K. Warburton, J. J. Kolata, and J. W. Olness, Phys. Rev. C **11**, 700 (1975).

[36] C. J. Chiara *et al.*, Phys. Rev. C **75**, 054305 (2007).